Computers & Geosciences 49 (2012) 290–296

Contents lists available at SciVerse ScienceDirect

Computers & Geosciences

journal homepage: www.elsevier.com/locate/cageo

An efficient finite volume model for shallow geothermal systems. Part I: Model formulation

M. Nabi *, R. Al-Khoury

Faculty of Civil Engineering and Geosciences, Delft University of Technology, The Netherlands

ARTICLE INFO

Article history:
Received 21 January 2012
Received in revised form
19 March 2012
Accepted 22 March 2012
Available online 2 April 2012

Keywords:
Ground-source heat pump
Borehole heat exchanger
BHE
Finite volume
Multigrid

ABSTRACT

This series of two papers presents a three-dimensional finite volume model for shallow geothermal systems. In this part, an efficient computational model describing heat and fluid flow in ground-source heat pumps is formulated. The physical system is decomposed into two subdomains, one representing a soil mass, and another representing one or a set of borehole heat exchangers. Optimization of the computational procedure has been achieved by, first, using a pseudo three-dimensional line element for modeling the borehole heat exchanger, and second, using a combination of a locally refined Cartesian grid and a multigrid with hierarchal tree data structure for discretizing and solving the soil mass governing equations. This optimization made the model computationally efficient and capable of simulating multiple borehole heat exchangers embedded in a multilayer system, in relatively short CPU time. In Part II of this series, verifications and numerical examples describing the computational capabilities of the model are presented.

1. Introduction

Geothermal heat is a renewable source of energy generated in the core of the earth, about 6000 km below the surface. Geothermal energy offers a number of advantages over conventional fossil-fuel resources, particularly the geothermal heat resources are locally available, renewable, economic, and their environmental impact in terms of CO_2 emissions is significantly lower. Deep geothermal resources have been exploited for the production of electricity and other direct uses (Bertani, 2005). Shallow geothermal resources have been widely used for direct uses, mainly space and greenhouse heating purposes (Lund et al., 2005). In this contribution, focus is placed on shallow geothermal systems, mainly the ground-source heat pumps.

Currently, different numerical methods have been utilized for the simulation of shallow geothermal systems. The finite difference method seems to dominate this research field, as it is traditionally utilized to solve heat flow problems. It is employed by Eskilson and Claesson (1988), Clauser (2002), Sliwa and Gonet (2005), Lee and Lam (2008), among others. The finite element method is recently gaining momentum and seems to be first employed by Muraya (1994), followed by, among others, Al-Khoury et al. (2005, 2010), Al-Khoury and Bonnier (2006), Marcotte and Pasquier (2008), Diersch et al. (2011a,b) and Raymond et al. (2011). The finite volume method has also been utilized to model ground-source heat exchangers. One of the earlier works in this field is that by Yavuzturk (1999), who developed a two-dimensional, fully implicit finite volume model using an automated parametric grid generation algorithm for different pipe sizes, shank spacing and borehole geometry. Rees et al. (2004) used the finite volume method to develop an axial-symmetric BHE-soil with groundwater flow model. This model was later extended and utilized by He et al. (2011) to simulate three-dimensional ground-source heat pumps. A multi-block structured mesh is used in this model, allowing the simulation of complex geometry around the borehole heat exchangers (BHE).

Most efforts for developing numerical models for shallow geothermal systems are spent on tackling two main issues: disproportional geometry and heat convection. Shallow geothermal systems, particularly vertical ground-source heat pumps, consist of very slender borehole heat exchangers (BHE) embedded in a vast soil mass. This geometrical peculiarity exerts enormous computational burden, as a combination of very fine elements (cells) and coarse elements (cells) is normally needed to discretize the computational domain. For three-dimensional systems, this normally requires hundreds of thousands to millions of elements, making the CPU time unrealistic for engineering purposes. This problem exuberates in the presence of convection and groundwater flow. Governing equations of cases with relatively high Peclet numbers behave like hyperbolic functions, which require fine meshes (grids) and proper upwind schemes. Different solutions have been proposed in literature for tackling these

* Correspondence to: Delft University of Technology, Stevinweg 1, 2628 CN, Delft, The Netherlands. Tel.: +31 641626133.
E-mail address: M.Nabi@tudelft.nl (M. Nabi).

0098-3004/$ - see front matter © 2012 Elsevier Ltd. All rights reserved.
http://dx.doi.org/10.1016/j.cageo.2012.03.019

problems. Here, we utilize the numerical model proposed by Al-Khoury et al. (2005), Al-Khoury and Bonnier, (2006).

In this contribution, a three-dimensional finite volume model for heat and fluid flow in ground-source heat pumps is formulated. A structured locally refined grid is utilized for the discretization of the spatial domain, and the theta method for the discretization of the temporal domain. The physical model is decomposed into two subdomains, one representing the soil mass, and the other representing one or more borehole heat exchangers. The soil mass is simulated as a fully saturated porous medium with groundwater flow, and the BHE is modeled using a pseudo three-dimensional line element. The thermal interaction between the BHE and soil mass is calculated sequentially by considering each one of them as a heat source to the other one, located at the contact surface between them.

In the following, governing equations representing the initial and boundary value problem of typical ground-source heat pumps are given. Then, a detailed formulation of the corresponding finite volume model is described. Later, a solution algorithm is outlined.

2. Governing equations

Governing equations of a shallow geothermal system, in particular, a ground-source heat pump, comprise heat equations and initial and boundary conditions of a soil mass and a borehole heat exchanger. The governing equations of the soil mass include also the continuity equation of the groundwater flow.

2.1. Soil heat and continuity equations

Heat transfer in a shallow geothermal system arises from the thermal interaction between the borehole heat exchangers and the soil mass. In a one-phase soil mass, constituting a solid skeleton, heat is merely conductive, while in the presence of groundwater flow, the soil mass constitutes a multiphase porous medium and the heat flow in this case is conductive-convective. In typical shallow geothermal systems, it is reasonable to assume that the groundwater flow is steady-state, and occurs in confined fully saturated soil layers. Furthermore, the groundwater flow is independent of temperature, but the temperature of the soil is highly dependent on the groundwater flow.

In the presence of groundwater, the transient heat flow balance equation of a soil mass can be described as

$$\rho c\frac{\partial T}{\partial t}=\nabla(\boldsymbol{\lambda}\nabla T)-\nabla(\rho_w c_w \mathbf{v}T)+H(x,y,z) \tag{1}$$

in which the subscript w refers to water, ρc (J/m^3 K) is the volumetric heat capacity, with ρ (kg/m^3) the mass density and c (J/kg K) the specific heat capacity, $\boldsymbol{\lambda}$ (W/m K) is the thermal conductivity tensor, $\mathbf{v}$ (m/s) is the Darcy velocity vector and $H(x,y,z)$ is a heat source. In practice, $\boldsymbol{\lambda}=\lambda_x=\lambda_y=\lambda_z=\lambda$, and for a two-phase material, the thermal conductivity and the volumetric heat capacity are described in terms of a local volume average, as

$$\begin{aligned}\lambda&=(1-n)\lambda_s+n\lambda_w\\ \rho c&=(1-n)\rho c_s+n\rho c_w\end{aligned} \tag{2}$$

where the subscript s refers to solid, and n is the material porosity. The Darcy velocity vector can be described as

$$\mathbf{v}=-\mathbf{k}\,\nabla\varphi \tag{3}$$

in which $\mathbf{k}=(\tilde{\mathbf{k}}\rho g/\mu)$ is the hydraulic conductivity tensor, commonly termed permeability (m/s), where $\tilde{\mathbf{k}}$ (m^2) is the intrinsic permeability tensor, μ (kg/ms) is the dynamic viscosity, and g (m/s^2) is the gravity. In engineering practice, $\boldsymbol{k}=k_x=k_y=k_z=k$. φ (m) in Eq. (3) is the total head, defined as

$$\varphi=\frac{P}{\rho g}+z \tag{4}$$

where $P/\rho g$ is the pressure head and z is the elevation head. The fluid flow balance equation, describing groundwater flow, is expressed as

$$S\frac{\partial\varphi}{\partial t}=-\nabla(\mathbf{k}\varphi)+Q(x,y,z) \tag{5}$$

in which S (m^{-1}) is the specific storage coefficient, which represents the amount of water released per unit area per head gradient and $Q(x,y,z)$ is a source or a sink.

2.1.1. Soil initial and boundary conditions

For the fluid flow, the initial condition in the soil mass, at time $t=0$, is described in terms of the hydrostatic head as

$$\varphi(x,y,z,0)=\varphi_0(x,y,z) \tag{6}$$

The boundary conditions for groundwater flow is most likely associated with a head difference between an upper stream and a lower stream occurring in a confined aquifer, described as

$$\begin{aligned}&\varphi(x=0,y,z)=\varphi_1, && \text{on } x=0 \text{ surface}\\ &\varphi(x=L,y,z)=\varphi_2, && \text{on } x=L \text{ surface}\\ &\mathbf{k}\nabla\varphi\,\mathbf{n}=J, && \text{on any of the boundary surfaces}\end{aligned} \tag{7}$$

in which L is the length (along the x-axis) of the distance between two known hydraulic heads, and J is a fluid flux.

For the heat flow, the initial condition of the soil mass, at time $t=0$, is defined as the steady-state condition

$$T(x,y,z,0)=f(x,y,z) \tag{8}$$

Boundary conditions associated with a shallow geothermal field might be:

$$\begin{aligned}&T(\mathbf{x},t)=f(\boldsymbol{x},t), && \text{on a point or a surface } \boldsymbol{x}\\ &\boldsymbol{\lambda}\nabla T\mathbf{n}=b_{as}(T_s-T_a), && \text{on the surface in contact with the air}\\ &\boldsymbol{\lambda}\frac{\partial T}{\partial n}=b_{gs}(T_s-T_g), && \text{on the surface in contact with a BHE}\end{aligned} \tag{9}$$

in which T_a is the air temperature, b_{as} is the convective heat transfer coefficient at the surface in contact with the air, T_g is the pipe (grout) temperature and b_{gs} is the reciprocal of the thermal resistance between the soil and the grout (borehole).

2.2. Borehole heat exchanger heat equations

Heat transfer in a borehole heat exchanger is conductive-convective and arises from the flow of a working fluid (refrigerant) circulating the pipes, and the thermal interaction between the borehole components and the surrounding soil mass. Heat transfer equations of a typical single U-tube BHE consisting of a pipe-in (denoted as i), a pipe-out (denoted as o), and a grout (denoted as g) can be described as (Al-Khoury, 2006)

Pipe-in

$$\rho c_r\frac{\partial T_i}{\partial t}-\lambda_r\frac{\partial^2 T_i}{\partial z^2}+\rho c_r u\frac{\partial T_i}{\partial z}=b_{ig}(T_g-T_i) \tag{10}$$

Pipe-out

$$\rho c_r\frac{\partial T_o}{\partial t}-\lambda_r\frac{\partial^2 T_o}{\partial z^2}-\rho c_r u\frac{\partial T_o}{\partial z}=b_{og}(T_g-T_o) \tag{11}$$

Grout

$$\rho c_g\frac{\partial T_g}{\partial t}-\lambda_g\frac{\partial^2 T_g}{\partial z^2}=b_{ig}(T_i-T_g)+b_{og}(T_o-T_g)+b_{gs}(T_s-T_g) \tag{12}$$

in which the subscript r represents the working fluid (refrigerant), u denotes the fluid velocity, T_s is the soil temperature in contact with the grout, b_{ig} is the reciprocal of the thermal resistance between pipe-in and grout, b_{og} is the reciprocal of the thermal resistance between pipe-out and grout, and b_{gs} is the reciprocal of the thermal resistance between the soil and the grout. The left hand-side of Eqs. (10)–(12) act on the volume of the specific component, and the right-hand side act on the contact surface area between interacting components. For simplicity of notation the subscript r will not be used unless necessary. This formulation can be extended to other types of borehole heat exchangers. For this see Al-Khoury, 2012.

This formulation emphasizes that, as manifested physically, the thermal interaction between the BHE components occurs via the grout, which works as an intermediate medium, transferring heat from one pipe to another and vice versa. The inclusion of the thermal interaction in the mathematical model alleviates the need for three-dimensional finite volume spatial discretization of the component geometry and allows for the use of a one-dimensional discretization. Such a reduction in the spatial discretization reduces significantly the grid size, making the calculation computationally feasible.

2.2.1. BHE initial and boundary conditions

Initially, at $t=0$, the temperature in the borehole heat exchanger is equal to the steady-state temperature in the soil before the heating/cooling operation starts, i.e.

$$T_i(z,0)=T_o(z,0)=T_g(z,0)=T_s(z,0) \tag{13}$$

in which T_s is the soil temperature immediately around the borehole.

Boundary conditions typically involved in an operating BHE are of two types: Dirichlet and Neumann. In the first boundary condition, at the inlet of pipe-in, $z=0$, the temperature is equal to the fluid temperature at the moment it enters into pipe-in, that is

$$T_i(0,t)=T_{\text{in}}(t) \tag{14}$$

In the second boundary condition, at the outlet of pipe-out, $z=0$, the flux is described as

$$\frac{\partial T_o(0,t)}{\partial z}=0 \tag{15}$$

2.2.2. Heat transfer coefficients

Heat transfer coefficients can be calculated using three different methods: experimental, analytical or numerical, and analogy to thermal circuits (Al-Khoury, 2012). Here we use the analogy to the thermal circuits, namely the Y configuration. Following this configuration, heat transfer coefficients for pipe-in – grout and pipe-out – grout can described as

$$b_{ig}=\frac{1}{R_{ig}},\quad b_{og}=\frac{1}{R_{og}} \tag{16}$$

where

$$R_{ig}=R_{\text{convection}}+R_{\text{pipematerial}}=\frac{1}{r_o/r_i\bar{h}}+\frac{r_o\ln(r_o/r_i)}{\lambda_{\text{p}}} \tag{17}$$

is the pipe-in – grout thermal resistance, with r_i and r_o the inner and the outer radius of the pipe-in respectively, λ_{p} the thermal conductivity of the pipe-in material, and $\bar{h}=(\text{Nu}\,\lambda/D)$, where D is the inner diameter of the pipe, and Nu is the Nusselt Number, which can be defined as (http://en.wikipedia.org/wiki/Nusselt_number).

Laminar flow: For fully-developed internal laminar flow in cylindrical tubes, the Nusselt numbers are constant. For convection with constant surface heat flux, the Nusselt number is:

$$\text{Nu}=4.36 \tag{18}$$

For convection with constant surface temperature, the Nusselt number is:

$$\text{Nu}=3.66 \tag{19}$$

Turbulent flow: Gnielinski correlation for turbulent flow in tubes is:

$$\text{Nu}=\frac{(f/8)(\text{Re}-1000)\text{Pr}}{1+12.7(f/8)^{1/2}(\text{Pr}^{2/3}-1)},\quad \begin{matrix}0.5<\text{Pr}<200\\ 3000<\text{Re}<5\text{E}6\end{matrix} \tag{20}$$

where f is the Darcy friction factor defined, for smooth tubes, as

$$f=(0.79\ln(\text{Re})-1.64)^{-2} \tag{21}$$

Dittus-Boelter correlation for turbulent flow in tubes is:

$$\text{Nu}=0.023\,\text{Re}^{4/5}\text{Pr}^{n},\quad \begin{matrix}0.7<\text{Pr}<160\\ \text{Re}\geq 10\,000\\ L/D\geq 10\end{matrix} \tag{22}$$

where $n=0.4$ for heating and $n=0.3$ for cooling, Pr is the Prandtl number and Re is the Reynolds number defined as $\text{Re}\equiv(uD_i/v)$, with u(m/s) the average refrigerant velocity, and $v\equiv(\mu_m/\rho)$ the kinematics viscosity (m^2/s) with μ_m (N s/m^2) the refrigerant mass-based viscosity and ρ (kg/m^3) its mass density. In the literature, the motion is usually considered turbulent for $\text{Re}>2000$. In practice Dittus-Boelter is used for smooth pipes.

Sieder–Tate correlation for turbulent flow in tubes is:

$$\text{Nu}=0.027\text{Re}^{4/5}\text{Pr}^{1/3}\left(\frac{\mu}{\mu_s}\right)^{0.14},\quad \begin{matrix}0.7<\text{Pr}<16\,700\\ \text{Re}\geq 10\,000\\ L/D\geq 10\end{matrix} \tag{23}$$

where μ is the fluid viscosity at the bulk fluid temperature, and μ_s is the fluid viscosity at the heat transfer surface temperature. This correlation is implicit non-linear, since the fluid viscosity is a function of the fluid Nusselt number. It is accurate and valid for a wider range of applications.

The same formulation is valid for R_{og}.

The heat transfer coefficient for grout-soil is described as

$$b_{gs}=\frac{1}{R_{ig}+R_{og}+R_{gs}} \tag{24}$$

where R_{ig} is as described earlier (same is valid for R_{og}), and R_{gs} may take this form:

$$R_{gs}=\frac{r_g\ln(r_g/r_{eq})}{\lambda_g} \tag{25}$$

in which r_g is the radius of the grout (borehole), and $r_{\text{eq}}=\sqrt{r_{\text{in}}^2+r_{\text{out}}^2}$ (r_{in}=pipe-in radius and r_{out}=pipe-out radius).

3. Finite volume discretization

The finite volume method is a numerical technique used for solving partial differential equations, mainly those related to transport phenomena. One of the important features of the finite volume method, as compared to the finite difference method, is that it can be implemented in a structured or unstructured mesh. Also, unlike the finite element method, the boundary conditions in the finite volume method are not invasive, giving more stability to the numerical processes. In this section, the finite volume method is utilized to discretize the spatial and the temporal domains of the initial and boundary value problems outlined above.

3.1. Spatial and temporal discretization

Using the finite volume method, the volume integrals of the involved partial differential equations are transformed into surface integrals by means of the divergence theorem. These terms are evaluated as fluxes at the surfaces of each finite volume. As the flux entering a given volume is identical to that leaving, the resulting system of equations is locally conservative.

Here, derivatives of the convection terms are discretized using a weighted cell-centered-upwind second-order scheme, and derivatives of the diffusion terms are discretized using the conventional cell-centered scheme. The temperature and the velocity are discretized on a staggered grid, entailing that the temperature is located at the center of the cell and the velocity vector is located at its surfaces, Fig. 1. This figure shows upstream sides, denoted as w, and s, and their corresponding downstream sides, denoted as e and n. The upstream and the downstream in the z-direction, not shown in the figure, are denoted as t and b respectively.

3.1.1. 3D soil finite volume

3.1.1.1. Heat flow. The soil heat equation, Eq. (1), can be written in an integral form as

$$\int_V \left(\rho c \frac{\partial T}{\partial t} + \rho_w c_w (\nabla \mathbf{v} T) - \nabla(\boldsymbol{\lambda} \nabla T) - H\right) dV = 0 \tag{26}$$

where $\nabla \boldsymbol{v} T$ is in a conservative form that includes the continuity condition $\nabla \boldsymbol{v} = 0$, such that

$$\nabla \mathbf{v} T_s = \mathbf{v} \nabla T_s + \underbrace{T_s \nabla \mathbf{v}}_{=0} \tag{27}$$

Using the divergence theorem, the volume integral of the convection term is evaluated as

$$\int_V \nabla \mathbf{v}\, T\, dV = \int_S \mathbf{v}\, T\, \mathbf{n}\, dS \tag{28}$$

Integrating the individual components of Eq. (28), and following the notation in Fig. 1, gives

$$\int_V \frac{\partial uT}{\partial x} dV = \int_S uT n_x dS = (u_e T_e - u_w T_w)\Delta y \Delta z$$

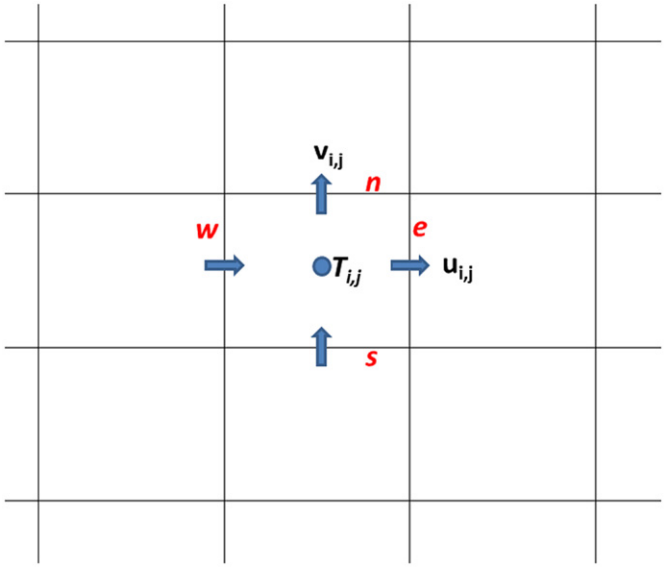

Fig. 1. Control volume.

$$\int_V \frac{\partial vT}{\partial y} dV = \int_S vT n_y dS = (v_n T_n - v_s T_s)\Delta x \Delta z$$
$$\int_V \frac{\partial wT}{\partial z} dV = \int_S wT n_z dS = (w_t T_t - w_b T_b)\Delta x \Delta y \tag{29}$$

where u, v and w are the Darcy velocity components along x, y and z axis respectively.

In a cell with a grid point (i,j,k) at the center, the right-hand side of Eq. (29) can be evaluated by weighted first order upwind and central difference, such that

$$\frac{\partial uT}{\partial x} = \alpha \left.\frac{\partial uT}{\partial x}\right|_{\text{upwind}} + (1-\alpha) \left.\frac{\partial uT}{\partial x}\right|_{\text{cen}} \tag{30}$$

in which α is a weighting factor. In e-w direction, this gives

$$\begin{aligned}(u_e T_e - u_w T_w)_{\text{upwind}} &= \frac{1}{2}\left[(u_e + |u_e|)T_{i,j,k} + (u_e - |u_e|)T_{i+1,j,k}\right. \\ &\quad \left. -(u_w + |u_w|)T_{i-1,j,k} - (u_w - |u_w|)T_{i,j,k}\right] \\ (u_e T_e - u_w T_w)_{\text{cen}} &= \frac{1}{2}\left[(T_{i,j,k} + T_{i+1,j,k})u_e - (T_{i,j,k} + T_{i-1,j,k})u_w\right]\end{aligned} \tag{31}$$

where $|u_e|$ represents the absolute value of u_e, etc.

Similarly, in n-s direction, gives

$$\begin{aligned}(v_n T_n - v_s T_s)_{\text{upwind}} &= \frac{1}{2}\left[(v_n + |v_n|)T_{i,j,k} + (v_n - |v_n|)T_{i,j+1,k}\right. \\ &\quad \left. -(v_s + |v_s|)T_{i,j-1,k} - (v_s - |v_s|)T_{i,j,k}\right] \\ (v_n T_n - v_s T_s)_{\text{cen}} &= \frac{1}{2}\left[(T_{i,j,k} + T_{i,j+1,k})v_n - (T_{i,j,k} + T_{i,j-1,k})v_s\right]\end{aligned} \tag{32}$$

In $t-b$ direction, it yields

$$\begin{aligned}(w_t T_t - w_b T_b)_{\text{upwind}} &= \frac{1}{2}\left[(w_t + |w_t|)T_{i,j,k} + (w_t - |w_t|)T_{i,j,k+1}\right. \\ &\quad \left. -(w_b + |w_b|)T_{i,j,k-1} - (w_b - |w_b|)T_{i,j,k}\right] \\ (w_t T_t - w_b T_b)_{\text{cen}} &= \frac{1}{2}\left[(T_{i,j,k} + T_{i,j,k+1})w_t - (T_{i,j,k} + T_{i,j,k-1})w_b\right]\end{aligned} \tag{33}$$

In the same way, the diffusion term $\nabla \cdot (\boldsymbol{\lambda} \nabla T)$ can be evaluated as

$$\int_V \lambda_x \frac{\partial^2 T}{\partial x^2} dV = \lambda_x \int_S \frac{\partial T}{\partial x} n_x dS = \lambda_x \left(\left.\frac{\partial T}{\partial x}\right|_e - \left.\frac{\partial T}{\partial x}\right|_w\right)\Delta y \Delta z \tag{34}$$

The partial derivatives on the right-hand side of Eq. (34) can be discretized using the central difference approximation, as

$$\begin{aligned}\left.\frac{\partial T}{\partial x}\right|_e &= \frac{T_{i+1,j,k} - T_{i,j,k}}{\Delta x} \\ \left.\frac{\partial T}{\partial x}\right|_w &= \frac{T_{i,j,k} - T_{i-1,j,k}}{\Delta x}\end{aligned} \tag{35}$$

Substituting Eq. (35) into Eq. (34) yields

$$\begin{aligned}\int_V \lambda_x \frac{\partial^2 T}{\partial x^2} dV &= \lambda_x \left(\frac{T_{i+1,j,k} - T_{i,j,k}}{\Delta x} - \frac{T_{i,j,k} - T_{i-1,j,k}}{\Delta x}\right)\Delta y \Delta z \\ &= \lambda_x \frac{T_{i+1,j,k} - 2T_{i,j,k} + T_{i-1,j,k}}{\Delta x}\Delta y \Delta z\end{aligned} \tag{36}$$

In the same way,

$$\int_V \lambda_y \frac{\partial^2 T}{\partial y^2} dV = \lambda_y \frac{T_{i,j+1,k} - 2T_{i,j,k} + T_{i,j-1,k}}{\Delta y}\Delta x \Delta z \tag{37}$$

$$\int_V \lambda_z \frac{\partial^2 T}{\partial z^2} dV = \lambda_z \frac{T_{i,j,k+1} - 2T_{i,j,k} + T_{i,j,k-1}}{\Delta z}\Delta x \Delta y \tag{38}$$

The volume integral of the temporal derivative in Eq. (26) can be evaluated as

$$\int_V \frac{\partial T}{\partial t} dV = \frac{\partial T}{\partial t} \Delta x \Delta y \Delta z \tag{39}$$

where the time derivative can be discretized as

$$\frac{\partial T}{\partial t} = \frac{1}{\Delta t}(T^{n+1} - T^n) \tag{40}$$

in which T^n is the value of T at time t and T^{n+1} is the value at time $t+\Delta t$, with Δt is the time step. The temperature and the heat source are evaluated in time using the theta-method as

$$\begin{aligned} T^{n+\theta} &= \theta T^{n+1} + (1-\theta) T^n \\ H^{n+\theta} &= \theta H^{n+1} + (1-\theta) H^n \end{aligned} \tag{41}$$

Putting Eqs. (30)–(40) together, using Eq. (41) and dividing by $\Delta V = \Delta x \Delta y \Delta z$ gives

$$\begin{aligned} &\rho c \frac{T^{n+1} - T^n}{\Delta t} + \rho_w c_w \left[\alpha \left(\frac{\partial uT}{\partial x} + \frac{\partial vT}{\partial y} + \frac{\partial wT}{\partial z} \right)_{\text{upwind}}^{n+\theta} \right. \\ &\quad \left. + (1-\alpha) \left(\frac{\partial uT}{\partial x} + \frac{\partial vT}{\partial y} + \frac{\partial wT}{\partial z} \right)_{\text{cen}}^{n+\theta} \right] - \left[\lambda_x \frac{T_{i+1,j,k} - 2T_{i,j,k} + T_{i-1,j,k}}{\Delta x^2} \right. \\ &\quad \left. + \lambda_y \frac{T_{i,j+1,k} - 2T_{i,j,k} + T_{i,j-1,k}}{\Delta y^2} + \lambda_z \frac{T_{i,j,k+1} - 2T_{i,j,k} + T_{i,j,k-1}}{\Delta z^2} \right]^{n+\theta} \\ &\quad + H_{i,j,k}^{n+\theta} = 0 \end{aligned} \tag{42}$$

where the derivative terms are described in Eqs. (30)–(33). $\theta = 0$ gives explicit scheme, $\theta = 1$ gives fully implicit, and $\theta = 1/2$ yields the Crank–Nicholson.

3.1.1.2. Groundwater flow. Evaluating the total head φ at the center of the cell, and using the discretization procedure outlined above, the finite volume equation of the groundwater flow, Eq. (5), can be described as

$$\begin{aligned} &S \frac{\varphi_{i,j,k}^{n+1} - \varphi_{i,j,k}^n}{\Delta t} + \frac{k_x}{\Delta x^2} (\varphi_{i+1,j,k} - 2\varphi_{i,j,k} + \varphi_{i-1,j,k})^{n+\theta} \\ &\quad + \frac{k_y}{\Delta y^2} (\varphi_{i,j+1,k} - 2\varphi_{i,j,k} + \varphi_{i,j-1,k})^{n+\theta} \\ &\quad + \frac{k_z}{\Delta z^2} (\varphi_{i,j,k+1} - 2\varphi_{i,j,k} + \varphi_{i,j,k-1})^{n+\theta} + Q_{i,j,k}^{n+\theta} = 0 \end{aligned} \tag{43}$$

The Darcy velocities are calculated as

$$\begin{aligned} u_{i,j,k} &= -k_x \frac{\varphi_{i+1,j,k} - \varphi_{i,j,k}}{\Delta x} \\ v_{i,j,k} &= -k_y \frac{\varphi_{i,j+1,k} - \varphi_{i,j,k}}{\Delta y} \\ w_{i,j,k} &= -k_z \frac{\varphi_{i,j,k+1} - \varphi_{i,j,k}}{\Delta z} \end{aligned} \tag{44}$$

3.1.2. Borehole heat exchanger finite volume

Using the discretization procedure for the convection term, Eq. (33), the diffusion term, Eq. (38) and the theta-method for the time integration, the finite volume equations of the borehole heat exchanger gives

Pipe-in

$$\begin{aligned} &\rho_r c_r \frac{T_k^{n+1} - T_k^n}{\Delta t}\bigg|_i + \rho_r c_r \left(\alpha \frac{\partial uT}{\partial z}\bigg|_{\text{upwind}} + (1-\alpha) \frac{\partial uT}{\partial z}\bigg|_{\text{cen}} \right)_i^{n+\theta} \\ &\quad - \lambda_r \left(\frac{T_{k+1} - 2T_k + T_{k-1}}{(\Delta z)^2} \right)_i^{n+\theta} \\ &\quad = b_{ig} (T_k|_g - T_k|_i)^{n+\theta} \end{aligned} \tag{45}$$

Pipe-out

$$\begin{aligned} &\rho_r c_r \frac{T_k^{n+1} - T_k^n}{\Delta t}\bigg|_o - \rho_r c_r \left(\alpha \frac{\partial uT}{\partial z}\bigg|_{\text{upwind}} + (1-\alpha) \frac{\partial uT}{\partial z}\bigg|_{\text{cen}} \right)_o^{n+\theta} \\ &\quad - \lambda_r \left(\frac{T_{k+1} - 2T_k + T_{k-1}}{(\Delta z)^2} \right)_o^{n+\theta} \\ &\quad = b_{og} (T_k|_g - T_k|_o)^{n+\theta} \end{aligned} \tag{46}$$

Grout

$$\begin{aligned} &\rho_g c_g \frac{T_k^{n+1} - T_k^n}{\Delta t}\bigg|_g - \lambda_r \left(\frac{T_{k+1} - 2T_k + T_{k-1}}{(\Delta z)^2} \right)_g^{n+\theta} \\ &\quad = b_{ig} (T_k|_i - T_k|_g)^{n+\theta} + b_{og} (T_k|_o - T_k|_g)^{n+\theta} + b_{sg} (T_s - T_k|_g)^{n+\theta} \end{aligned} \tag{47}$$

in which T_s denotes the soil temperature, and

$$\begin{aligned} \frac{\partial uT}{\partial z}\bigg|_{\text{upwind}} &= \frac{u_t T_t - u_b T_b}{\Delta z} = \frac{1}{\Delta z} \left[\frac{u_t + |u_t|}{2} T_k + \frac{u_t - |u_t|}{2} T_{k+1} \right. \\ &\quad \left. - \frac{u_b + |u_b|}{2} T_{k-1} - \frac{u_b - |u_b|}{2} T_k \right] \\ \frac{\partial uT}{\partial z}\bigg|_{\text{cen}} &= \frac{u_t T_t - u_b T_b}{\Delta z} = \frac{1}{\Delta z} \left[u_t \frac{T_k + T_{k+1}}{2} - u_b \frac{T_k + T_{k-1}}{2} \right] \end{aligned} \tag{48}$$

4. Solution algorithm

Finite volume discretization of the involved initial and boundary value problems of the soil mass and the borehole heat exchanger has resulted to two sets of coupled algebraic equations. These equations are linear and can be solved simultaneously using direct or iterative solvers. However, and as the governing equations are non-symmetric and relatively large for typical 3D shallow geothermal systems, a sequential algorithm is more feasible. In this work, the soil mass equations are solved iteratively using the multigrid scheme, and the borehole heat exchangers equations are solved using the direct Thomas algorithm. The two solution schemes are coupled using an iterative algorithm, outlined hereafter.

4.1. Solving borehole heat exchanger equations

Collecting terms in Eqs. (45)–(47) gives

$$a_k T_{k-1} + b_k T_k + c_k T_{k+1} = f_k \tag{49}$$

in which T represents pipe-in, pipe-out or grout temperatures, and a, b, c and f are coefficients defined as

Pipe-in

$$\begin{aligned} a_k &= \theta(C_2 - 2\alpha C_1 - (1-\alpha)C_1) \\ b_k &= \theta(C_0 + 2\alpha C_1 - 2C_2) + 1 \\ c_k &= \theta(C_2 + (1-\alpha)C_1) \\ f_k &= (1-\theta) \begin{bmatrix} C_0 (T_k^n|_g - T_k^n) - C_2 (T_{k-1}^n - 2T_k^n + T_{k+1}^n) \\ -2C_1 \alpha (T_k^n - T_{k-1}^n) - C_1 (1-\alpha)(T_{k+1}^n - T_{k-1}^n) \end{bmatrix} \\ &\quad + C_0 \theta T_k^{n+1}|_g + T_k^n \end{aligned} \tag{50}$$

where

$$C_0 = \frac{b_{ig} \Delta t}{\rho_r c_r} \frac{dS_{ig}}{dV_i}; \quad C_1 = \frac{u\, \Delta t}{2\, \Delta z_p}; \quad C_2 = -\frac{\lambda_r \Delta t}{\rho_r c_r \Delta z_p^2} \tag{51}$$

Pipe-out

Similar equations as those for pipe-in, with

$$C_0 = \frac{b_{og} \Delta t}{\rho_r c_r} \frac{dS_{og}}{dV_o}; \quad C_1 = -\frac{u\, \Delta t}{2 \Delta z_p}; \quad C_2 = -\frac{\lambda_r \Delta t}{\rho_r c_r \Delta z_p^2} \tag{52}$$

Grout

$$a_k = C_g\theta$$
$$b_k = (C_{g1}+C_{g2}+C_{g3}-2C_g)\theta+1$$
$$c_k = C_g\theta$$
$$f_k = (1-\theta)\begin{bmatrix} C_{g1}(T_o^n-T_k^n)+C_{g2}(T_i^n-T_k^n) \\ +C_{g3}(T_s^n-T_k^n)-C_g(T_{k-1}^n-2T_k^n+T_{k+1}^n)\end{bmatrix} + \theta[C_{g1}T_i^{n+1}+C_{g2}T_o^{n+1}+C_{g3}T_s^{n+1}]+T_k^n \quad (53)$$

where

$$C_{g1}=\frac{b_{ig}\Delta t}{\rho_g c_g}\frac{dS_{ig}}{dV_g};\quad C_{g2}=\frac{b_{og}\Delta t}{\rho_g c_g}\frac{dS_{og}}{dV_g}$$
$$C_{g3}=\frac{b_{gs}\Delta t}{\rho_g c_g}\frac{dS_{gs}}{dV_g};\quad C_g=-\frac{\lambda_g\Delta t}{\rho_g c_g\, dy_p^2} \quad (54)$$

Putting these equations together, a tridiagonal matrix is obtained, which can be solved by Thomas algorithm. This algorithm is a simplified Gaussian elimination suitable for tridiagonal systems of equations. As the thermal interactions between the borehole components are included in the differential equations, Eqs. (10)–(12), a one-dimensional (line) cell is sufficient to describe the heat flow. This reduces the computational cost significantly, making simulation of multiple borehole heat exchangers very feasible.

4.2. Solving soil equations

Computing the soil mass energy equation is the most time consuming in the current model. To minimize the computational cost, a combination between a locally refined grid and a geometric multigrid solver is adopted. The soil mass is discretized by a locally structured Cartesian grid using local refinements at regions with high gradients. This algorithm is highly economic, but the grid of this kind does not have a direct (i,j,k) structure, normally obtained from the standard structured Cartesian approach. In the proposed locally structured algorithm, the domain is first discretized using a relatively course grid. Then, cells at regions of interest are divided by eight sub-cells (four sub-cells in 2D), Fig. 2. The (i,j,k) structure is maintained, as shown below. This process can be repeated if more refinement is needed. Fig. 3 shows a sketch of a grid refinement near a point.

Computer coding of a grid consisting of a set of refined Cartesian cells is commonly managed in two ways: fully unstructured data structure or hierarchical tree data structure. In the fully unstructured technique, each cell, in a three-dimensional grid, is connected directly to one or four neighboring cells on each direction. A main drawback of this approach is that the stencil of discretization requires awkward interpolations between neighboring cells that might lead to highly disperse matrices, known in literature as discretization pollution (Trottenberg et al., 2001). To avoid this shortcoming, interpolations based on the least square method are employed. However, the use of such interpolations results to numerical instability, necessitating some sort of numerical limiters to damp the numerical oscillations. See, for example, Koh et al. (2003) and Berger et al. (2005).

The use of the hierarchical tree data structure is an important alternative. This technique results to a multi-level grid, where grids of different resolutions are generated and nested over each other, as shown in Fig. 4. The hierarchical tree structure provides a logical means of finding cell-to-cell connectivity and allows straightforward refinement and coarsening through tree growth and pruning (Coirier and Powell, 1996). The shortcoming of this technique, however, is that the calculation time required for the recursive routines necessary for the determination of cell-to-cell connectivity is relatively higher than that for the fully unstructured data structure.

To avoid the shortcomings of both techniques, in this work, an approach based on the multilevel adaptive refinement (MLAT) is adopted (Brandt, 1977). In this approach, the multi-level data structure of the hierarchical tree is utilized together with a locally structured connectivity. By such a data structure, the direct (i,j,k) grid connectivity is maintained and can be utilized to connect cells at a certain grid level. The parent-child tree structure can be utilized to connect grid cells at different levels. This scheme suites very well the multigrid concept.

Multigrid techniques are generally accepted as fast and efficient algorithms for solving many types of partial differential equations. They exhibit an optimal complexity and are, in theory, independent on the mesh size (Saad, 2003). In this work, the multigrid algorithm is utilized to solve the finite volume equations, discretized on the locally refined multi-level grid, described above. The computational efficiency is enhanced by coarsening the grid to the coarsest possible level, and the solution is conducted by either a V or a W multigrid cycle, a recursive procedure applied at each grid level as it moves through the grid hierarchy.

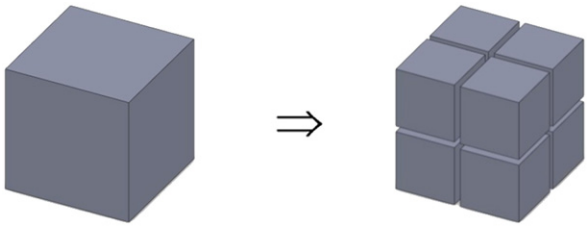

Fig. 2. 3D coarse (parent) cell divided into 8 fine (children) cells.

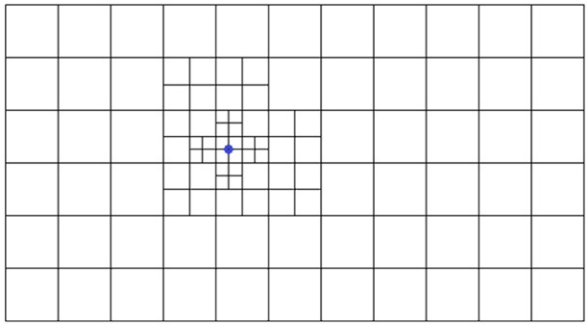

Fig. 3. Grid refinemet around a point.

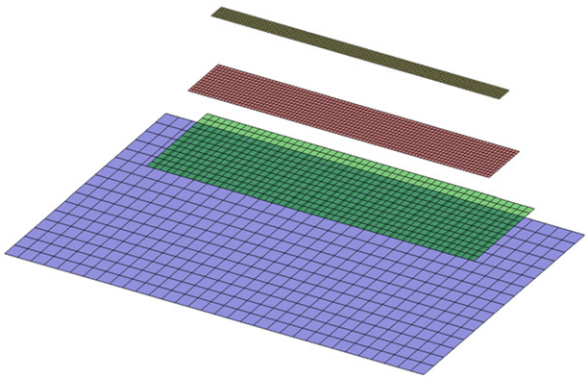

Fig. 4. A sketch of a multi-level grid.

One of the important aspects of a multigrid algorithm is the smoothing process. Here, we applied Gauss Seidel smoothing because of its simplicity, stability, and ability to damp high-frequency errors. A non-linear multigrid algorithm, namely the Full Approximation Storage (FAS) multigrid is applied. Even though the involved governing equations are linear, the use of a nonlinear multigrid algorithm is known to be highly stable, especially for problems with local refinement.

The efficiency of the multigrid methods degenerates significantly in the presence of anisotropy. This problem can be avoided by semi-coarsening techniques or by linewise smoothing (Trottenberg et al., 2001). In the present work, the linewise smoothing is applied because of its simplicity in programming. The linewise smoother keeps the standard multigrid coarsening, but changes the relaxation procedure from pointwise to linewise. That is, all unknowns on a line are updated collectively. The collective solution of all equations corresponding to a line leads to a solution of a tridiagonal system of equations, which can be solved by a direct and cost-efficient algorithm, such as Thomas algorithm.

Using local refinements in a Cartesian grid, the prescription of the boundary conditions needs to be mapped to the children cells. The boundary conditions at the fine grids are interpolated from their coarser grids. The order of interpolation has to be higher than the order of accuracy of the computational scheme (Trottenberg et al., 2001). At least a third order interpolation is required to conserve the second-order accuracy of the scheme. Here, a fifth order of interpolation is applied.

4.3. Sequential scheme

The discrete set of governing equations of a shallow geothermal system, represented by a soil mass and one or more borehole heat exchangers, is solved using a sequential scheme, described as

1. Solve the groundwater flow equation, and calculate Darcy velocity.
2. DO iteration
   - Solve the soil energy equation using the multigrid algorithm (iterative solver).
   - Identify the soil temperatures at contact surfaces with the BHEs, and include them to the source vectors of the BHEs.
   - Solve the BHEs energy equations using Thomas algorithm (direct solver).
   - Identify the grout temperatures and include them to the source vector of the soil mass at the contact surface areas with the BHEs.
   - Check the residual ($\|Ax-b\|/\|b\|$). If it is not converged, go to 2.

   END DO iteration
3. END SCHEME

5. Conclusions

In this contribution, a computationally efficient three-dimensional finite volume model for heat and fluid flow in a ground-source heat pump is formulated. Two main aspects have contributed to the computational efficiency: the borehole heat exchanger model, and the discretization technique. In the first aspect, heat flow in a borehole heat exchanger is modeled using a pseudo three-dimensional line element. By such a model, thermal interactions between the BHE components are included in the mathematical model, alleviating thus the need for geometrical discretization. In the second aspect, solution of the energy equation of the soil mass, which is the most CPU time consuming, is conducted via a combination of a structured locally refined grid and a hierarchal multigrid iterative solver. By such a grid and solver, computational efficiency and stability are gained. In Part II, the numerical accuracy and the computationally capabilities of the proposed model are elaborated.

References

Al-Khoury, R., 2012. Computational Modeling of Shallow Geothermal Systems. CRC press, Leiden, pp. 254.

Al-Khoury, R., Bonnier, P.G., Brinkgreve, B.J., 2005. Efficient finite element formulation for geothermal heating systems. Part I: steady state. International Journal for Numerical Methods in Engineering 63, 988–1013.

Al-Khoury, R., Bonnier, P.G., 2006. Efficient finite element formulation for geothermal heating systems. Part II: transient. International Journal for Numerical Methods in Engineering 67, 725–745.

Al-Khoury, R., Kolbel, T., Schramedei, R., 2010. Efficient numerical modelling of borehole heat exchangers. Computers and Geosciences 36, 1301–1315.

Berger, M., Aftosmis, M.J., Murman, S.M., 2005. Analysis of slope limiters on irregular grids. In: 43rd AIAA Aerospace Sciences Meeting, Reno, NV.

Bertani, R., 2005. World geothermal power generation in the period 2001–2005. Geothermics 34, 651–690.

Brandt, A., 1977. Multi-level adaptive solutions to boundary-value problems. Mathematics of Computation 31, 333–390.

Clauser, C., 2002. Numerical Simulation of Reactive Flow in Hot Aquifers. SHEMAT and Processing SHEMAT. Springer 2003.

Coirier, W.J., Powell, K.G., 1996. Solution-adaptive Cartesian cell approach for viscous and inviscid flows. AIAA Journal 34, 938–945.

Diersch, H.-J.G., Bauer, D., Heidemann, W., Rühaak, W., Schätzl, P., 2011a. Finite element modeling of borehole heat exchanger systems—Part 1. Fundamentals. Computers and Geosciences 37 (8), 1122–1135.

Diersch, H.-J.G., Bauer, D., Heidemann, W., Rühaak, W., Schätzl, P., 2011b. Finite element modeling of borehole heat exchanger systems—Part 2. Numerical simulation. Computers and Geosciences 37 (8), 1136–1147.

Eskilson, P., Claesson, J., 1988. Simulation model for thermally interacting heat extraction boreholes. Numerical Heat Transfer 13, 149–165.

He, M., Rees, S., Shao, L., 2011. Simulation of a domestic ground source heat pump system using a transient numerical borehole heat exchanger model. Journal of Building Performance Simulation 4 (2), 141–155.

Koh, E.P.C., Tsai, H.M., Liu, F., 2003. Euler solution using Cartesian grid with least squares technique. In: 41th AIAA Aerospace Sciences Meeting and Exhibit, AIAA-2003-1120, Reno, Nevada.

Lee, C.K., Lam, N.H., 2008. Computer simulation of borehole ground heat exchangers for geothermal heat pump systems. Renewable Energy 33 (6), 1286–1296.

Lund, J.W., Freeston, D.H., Boyd, T.L., 2005. Direct application of geothermal energy: 2005 worldwide review. Geothermics 34, 691–727.

Marcotte, D., Pasquier, P., 2008. Fast fluid and ground temperature computation for geothermal ground-loop heat exchanger systems. Geothermics 37 (6), 651–665.

Muraya, N.K., 1994. Numerical modelling of the transient thermal interface of vertical U-tube heat exchangers. Ph.D. Dissertation, Texas A&M University, USA, 185 pp.

Raymond, J., Therrien, R., Gosselin, L., 2011. Borehole temperature evolution during thermal response tests. Geothermics 40 (1), 69–78.

Rees, S.J., Spitler, J.D., Deng, Z., Orio, C.D., Johnson, C.N., 2004. A study of geothermal heat pump and standing column well performance. ASHRAE Transactions 110 (1), 3–13.

Saad, Y., 2003. Iterative Methods for Sparse Linear Systems. SIAM.

Sliwa, T., Gonet, A., 2005. Theoretical model of borehole heat exchanger. Journal of Energy Resources Technology, ASME 27, 142–148.

Trottenberg, U., Oosterlee, C.W., Schüller, A., 2001. MULTIGRID. Academic Press.

Yavuzturk, C., 1999. Modeling of vertical ground loop heat exchangers for ground source heat pump systems. Ph.D. Dissertation, Oklahoma State University, USA, 231 pp.